Entanglement transition and replica wormholes in the dissipative Sachdev-Ye-Kitaev model

Hanteng Wang,[1,*] Chang Liu,[1,†] Pengfei Zhang,[2,‡] and Antonio M. García-García[1,§]

[1]*Shanghai Center for Complex Physics, School of Physics and Astronomy, Shanghai Jiao Tong University, Shanghai 200240, China*

[2]*Department of Physics, Fudan University, Shanghai, 200438, China*

(Received 27 June 2023; accepted 16 January 2024; published 8 February 2024)

Recent discoveries have highlighted the significance of replica wormholes in resolving the information paradox and establishing the unitarity of black hole evaporation. In this paper, we propose the dissipative Sachdev-Ye-Kitaev (SYK) model as a minimal quantum model that exhibits entanglement dynamics with features qualitatively similar to replica wormholes. As a demonstration, we investigate the entanglement growth of a pair of dissipative SYK models initialized in a thermofield double state. In the regime of large N with weak dissipation, we observe a first-order entanglement transition characterized by a switch of the dominant saddle point: from replica-diagonal solutions for short times to replica wormholelike off-diagonal solutions for long times. Furthermore, we show that the signature of replica wormholes persists even at moderate $N \lesssim 30$ by using the Monte Carlo quantum trajectory method. Our work may pave the way for explorations of replica wormhole physics in quantum simulators.

DOI: 10.1103/PhysRevD.109.046005

I. INTRODUCTION

Recently, there has been growing interest in comprehending systems with nonunitary dynamics. Experimental investigations into PT-symmetry breaking of non-Hermitian Hamiltonians have been conducted in the field of quantum optics [1] and cold atoms [2]. Additionally, numerous theoretical predictions have been made, encompassing studies of information flow [3], non-Hermitian superconductivity [4], and particle detectors [5]. Significant progress has also been achieved on the role of dissipation in quantum many-body dynamics [6–11], which unveils enriched symmetry classes [12–15]. Moreover, the nonunitarity can drive dynamical transitions when following quantum trajectories [16–19] or maintaining access to different environments [20,21].

Interestingly, the study of nonunitary dynamics is gaining traction in a completely different field: quantum gravity. On the one hand, this benefits from the existence of a low-energy duality between the Sachdev-Ye-Kitaev (SYK) model [22–25] and Jackiw-Teitelboim gravity [26–29], which enables the study of black holes and wormholes in concrete quantum systems [30–40]. On the other hand, the coupling of black holes to an environment is naturally connected with the so-called information paradox [41]. Recent advancements in resolving this paradox have led to the identification of a new Ryu-Takayanagi surface [42–44], which includes entanglement islands linked to complex structures known as replica wormholes [45–47]. These wormholes, central to our study, are conceptualized as spacetime structures that connect different "replicas" of a quantum system. They play a crucial role in resolving the information paradox, suggesting that entanglement in quantum gravity might be geometrically manifested as wormholes, leading to a first-order Page transition [48] in the growth of entanglement. Remarkably, similar phenomena have been observed in SYK models, particularly where the environment is modeled as a Majorana chain [49].

With SYK-like models now implemented on quantum simulation platforms [50,51], SYK systems coupled to environments emerge as prime candidates for observing replica wormholes. The SYK model characterized by its chaotic dynamics and substantial entanglement mirrors the intricate entanglement structures prevalent in black holes. This parallel is drawn through its capacity to exhibit off-diagonal replica structures [35,52]. However, existing models integrating microscopic baths [49,53–55] pose challenges for quantum simulations due to their demands for additional logical qubits.

II. MODEL AND NOTIONS

We consider a pair of q-body SYK models with identical internal couplings denoted by L and R. Each of them is described by the Hamiltonian,

*hantengwang.physics@gmail.com
†cl91tp@gmail.com
‡pengfeizhang.physics@gmail.com
§amgg@sjtu.edu.cn

$$H = \sum_{1\le i_1<i_2<\ldots<i_q\le N} \mathrm{i}^{q/2} J_{i_1 i_2 \ldots i_q} \chi_{i_1}\chi_{i_2}\cdots\chi_{i_q}, \tag{1}$$

where N is the number of Majoranas defined by $\{\chi_i,\chi_j\}=\delta_{ij}$, $J_{i_1 i_2\ldots i_q}$ are Gaussian-independent random couplings with zero mean and variance $\langle J^2_{i_1 i_2\ldots i_q}\rangle_{\mathrm{dis}} = (q-1)!J^2/N^{q-1}$, and i denotes the imaginary unit. The single-sided SYK Hamiltonian H has $2^{N/2}$ eigenstates $|n\rangle$ with energies E_n. The full two-sided Hamiltonian of the system can be represented as $H_{\mathrm{S}} = H_{\mathrm{L}} + H_{\mathrm{R}} = H\otimes\mathbb{I} + \mathbb{I}\otimes H^T$. The L-R systems are initially highly entangled and prepared in a TFD state with inverse temperature β in the form [56]

$$|\Psi(t=0)\rangle = |\mathrm{TFD}_\beta\rangle = Z_\beta^{-1/2} e^{-\frac{\beta}{4}(H_{\mathrm{L}}+H_{\mathrm{R}})}|I\rangle, \tag{2}$$

where $|I\rangle$ is the maximally entangled state satisfying $\chi_{i,\mathrm{L}}|I\rangle = -\mathrm{i}\chi_{i,\mathrm{R}}|I\rangle$ [36,57]. The single SYK thermal partition function $Z_\beta = \mathrm{Tr}(e^{-\beta H})$ serves as the normalization.

The growth of entanglement has also been studied in SYK-like systems [57–66], including in studies of measurement-induced phase transitions [67–71]. However, most of these works focus on closed systems or microscopic environment models. In this paper, we instead consider a Markovian environment [37–39], which results in the Lindbladian form of the density matrix $\mathcal{P}(t)$ time evolution:

$$\partial_t\mathcal{P} = -\mathrm{i}[H_{\mathrm{S}},\mathcal{P}] + \sum_i^N \sum_{x=\mathrm{L,R}} \left[L_{x,i}\mathcal{P}L_{x,i}^\dagger - \frac{1}{2}\{\mathcal{P}, L_{x,i}^\dagger L_{x,i}\}\right], \tag{3}$$

with jump operators $L_{\mathrm{L},i} = \sqrt{\mu}\chi_{\mathrm{L},i}$ and $L_{\mathrm{R},i} = \sqrt{\mu}\chi_{\mathrm{R},i}$. The coupling strength μ between the systems and their environment is identical for all sites i.

The aim of this work is to study the dynamical entanglement structure of this dissipative SYK model with TFD initial states by calculating its second Rényi entropy $S = -\langle \ln\gamma\rangle_{\mathrm{dis}}$, where $\gamma(t) = \frac{\mathrm{Tr}(\mathcal{P}^2)}{(\mathrm{Tr}\mathcal{P})^2}$ is called purity, and $\langle\cdots\rangle_{\mathrm{dis}}$ denotes an average over different realizations of SYKs. For the sake of simplicity, we use an unnormalized density matrix $\mathrm{Tr}\mathcal{P} = Z_\beta$. Because of the self-averaging feature of the SYK model [25,52,72,73], we compute annealed instead of quenched averages, i.e., $S \approx -\ln\langle\gamma\rangle_{\mathrm{dis}}$.

III. PATH INTEGRAL FOR PURITY

We use the Keldysh path integral formulation [74–76] to evaluate the dynamics of the unnormalized purity $\mathrm{Tr}(\mathcal{P}^2)$. We introduce two replicas, a and b. As a result, four distinct time contours are needed, defined as u_+^a, u_-^a, u_+^b, and u_-^b, which can be compactified in terms of a single time variable

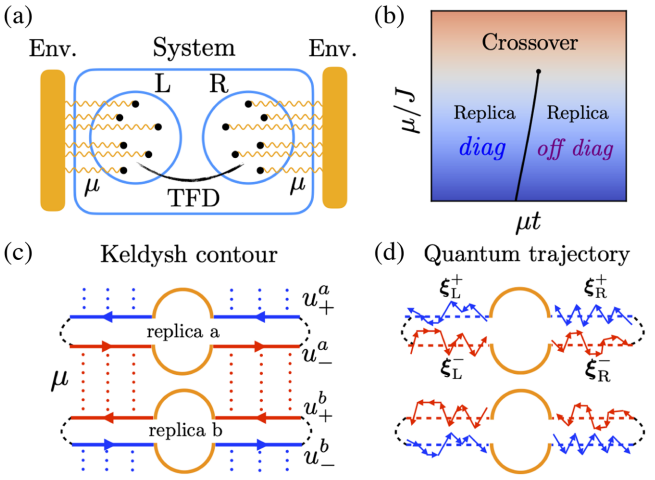

FIG. 1. (a) Illustration of the setup. L and R systems are entangled without direct interaction between them. (b) Dynamical phase diagram of the system. The x axis stands for real time in units of $1/\mu$, and the y axis stands for the coupling strength μ in unit of J. (c) Sketch of the purity calculation in replica a, b with four time contours u_+^a, u_-^a, u_+^b, and u_-^b connected by the Lindbladian coupling μ. (d) An example of a quantum trajectory employed in the purity calculation at finite N.

u as illustrated in Fig. 1(c). As a result, $\mathrm{Tr}(\mathcal{P}^2)$ reads (see Appendix A for derivation)

$$\mathrm{Tr}(\mathcal{P}^2) = \int \mathcal{D}\chi \exp\left\{-\int_{\mathcal{C}} du\left[\frac{1}{2}\sum_i^N \chi_i\partial_u\chi_i + f(u)H\right] + \mu\int du \sum_i^N \sum_{\eta\neq\eta'} \chi_i(u_\eta^a)\chi_i(u_{\eta'}^b) - 2\mu N t\right\}. \tag{4}$$

The first line in the exponential represents the unitary evolution where $f(u) = \mathrm{i}, -\mathrm{i}, 1$ corresponds to forward (+), backward (−), and rotational (imaginary) evolution contours, respectively. Meanwhile, the second line describes the effect of the environment modeled by nonunitary interactions between replicas on forward and backward contours.

The next step is to integrate over disorder and express the path integral in terms of the Green's function $G(u,u') = \frac{1}{N}\sum_i \chi_i(u)\chi_i(u')$ and the corresponding Lagrange multiplier, $\Sigma(u,u')$ [24]. After performing the average over random couplings, standard SYK techniques lead to $\langle \mathrm{Tr}[\mathcal{P}(t)^m]\rangle_{\mathrm{dis}} = \int \mathcal{D}G\mathcal{D}\Sigma e^{-S_{\mathrm{eff}}^{(m)}[G,\Sigma]}$, as sketched in Appendix A. In the large N limit, the saddle-point approximation can be utilized. The final expression for the large N second Rényi entropy is computed from the on-shell $G-\Sigma$ action $S = S_{\mathrm{eff}}^{(2)}[\mathcal{G},\Sigma] - 2S_{\mathrm{eff}}^{(1)}[\mathcal{G},\Sigma]$, with $\mathcal{G}$ and Σ the solutions of the corresponding Schwinger-Dyson equations.

A. Large N numerics

Except in the large-q limit, the saddle-point equations can only be solved numerically by discretizing each time contour into $\mathcal{N}$ segments of length δt. Then, $G(u,u')$ and $\Sigma(u,u')$ are computed by solving iteratively the resulting discrete matrix equations as discussed in Appendix A. For the initial state with $\beta J = 0$, there exist two distinct types of saddle-point solutions for G: the replica diagonal in the a, b space [left panel of Fig. 2(a)], and the replica off-diagonal configuration [right panel of Fig. 2(a)]. At short times and small μ/J, only the replica-diagonal solution is present. In this region, $G^{ab} \approx G_0 \propto \delta^{a,b}$ and we find that the Rényi entropy is given by $2\mu N t$. The off-diagonal components $\sim \mu t$ (see left panel of Fig. 2) are subleading at this moment. This solution cannot dominate for $t \gg 1/\mu$ because the entropy would grow indefinitely, leading to the equivalent issue of the information paradox in gravity [77]. Indeed, we have identified (see Fig. 3) a Page time [$\mu t \sim \mathcal{O}(1)$], at which the replica-off-diagonal, in the a, b space, solution becomes dominant. This switch of saddles at the Page time prevents the entropy from growing forever. Instead, as depicted in Fig. 3(a), it saturates at $N \ln 2$. This indicates that the system, when thermalized to infinite temperature, can be approximated as two independent SYK dots. For detailed information, see Appendixes A and B. The short- and long-time phases are clearly separated by a first-order entanglement transition in the small μ/J regime. This late-time saddle is very similar to the replica wormhole reported in gravity [45,46].

On the other hand, the transition turns into a crossover for large μ/J values. This phenomenon can be attributed to the absence of a significant symmetry difference between the two phases. For small μ/J, it is possible to distinguish the two phases based on the magnitude of the off-diagonal components, which are either large, of order $\mathcal{O}(1)$, or small, of order $\mathcal{O}(\mu/J)$. However, for large μ/J, the off-diagonal components no longer exhibit such a difference, leading to a hybridized and smooth behavior that results in a crossover instead of a sharp transition. By examining the derivative of the Rényi entropy, it becomes apparent that there is a noticeable gap when $\mu < \mu_c \approx 0.156J$, and the gap closes when $\mu > \mu_c$; see Fig. 3(b) and its inset. These observations hold true for the large βJ case as well; see Appendix A for a detailed account.

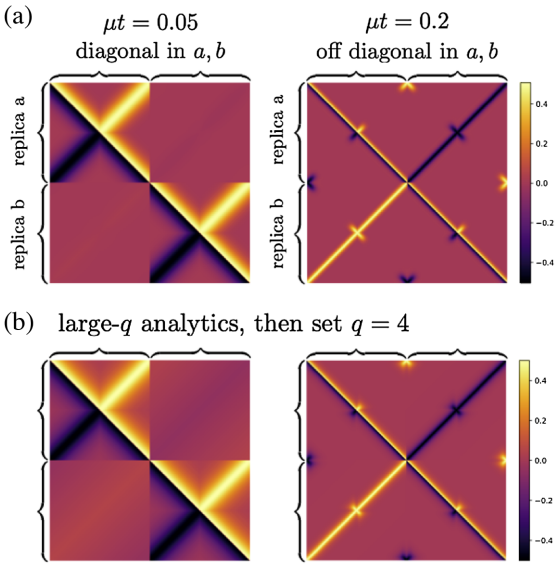

FIG. 2. (a) Large N, $q = 4$ numerical Green's function. Two types of saddle-point solutions: replica-diagonal (left panel) vs replica-off-diagonal (right panel) solutions with $\mu = 0.01J$. (b) Large-q analytical results.

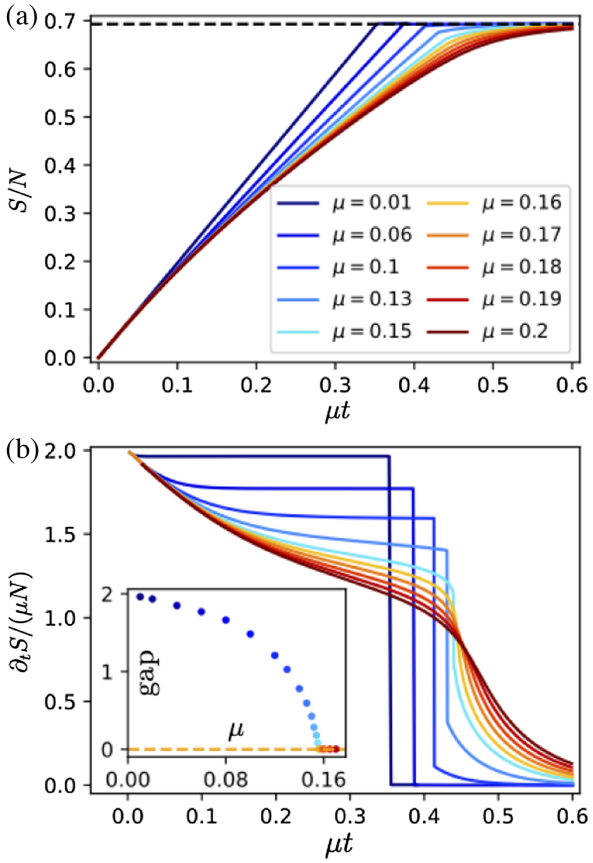

FIG. 3. (a) Large N Page curve for an initial $\beta J = 0$ TFD state, with μ values ranging from $0.01J$ to $0.2J$. (b) Derivative of Rényi entropy with respect to time, i.e., $\frac{1}{\mu N}\partial_t S$. Inset: gap of $\frac{1}{\mu N}\partial_t S$ at Page time vs μ/J. A first-order entanglement transition at the Page time is only observed for $\mu \lesssim 0.156J$. We set $J = 1$ in all numerical results.

B. Large-q analytical solution

In the large-q limit, it is possible to compute the Green's functions analytically [24]. We define scaled couplings $\mathcal{J}^2 = qJ^2/2^{q-1}$, $\hat{\mu} = q\mu$ which are fixed in the large-q limit. The Green's functions are denoted by $G^{aa}_{\eta\eta'} \equiv G(u^a_\eta, u^a_{\eta'})$ and $G^{ab}_{\eta\eta'} \equiv G(u^a_\eta, u^b_{\eta'})$, where η, η' stands for

forward/backward $\pm$. The difference between the two time arguments is $\Delta u \equiv u - u'$. For simplicity, we focus again on the $\beta J = 0$ case.

At short times $\hat{\mu}t \ll q$, the contribution from finite μ is perturbative. To leading order in $\hat{\mu}/\mathcal{J}$, the Green's function within each replica can be approximated by the equilibrium solution with $\hat{\mu} = 0$: $G^{aa}_{\eta\eta'} = \frac{G_{0,\eta\eta'}(\Delta u)}{\cosh^{2/q}(\mathcal{J}\Delta u)}$. Inter-replica Green's functions involve the convolution of two $G^{aa}_{\eta\eta'}$'s, and to lowest order it gives

$$G^{ba}_{\eta\eta'} = \frac{\hat{\mu}}{2q}\begin{pmatrix} u+u'-2t & 2t-|\Delta u| \\ 2t-|\Delta u| & u+u'-2t \end{pmatrix}, \tag{5}$$

which becomes large enough at sufficiently long time $t \sim q/\hat{\mu}$, where perturbation theory breakdown. By computing the on-shell action, it is straightforward to show that Eq. (5) results in $S \approx 2\hat{\mu}Nt/q$, consistent with the previous perturbative result.

On the other hand, in the long-time limit $\hat{\mu}t \to \infty$, the pairing between branches changes, and the solution is replica off diagonal. The Green's functions can be approximated by the "factorization of twist operators" [49]. We first consider the Green's functions where two fermion operators are inserted in branches $\mathcal{C}_{\text{red}} = (b,+) \cup (a,-)$:

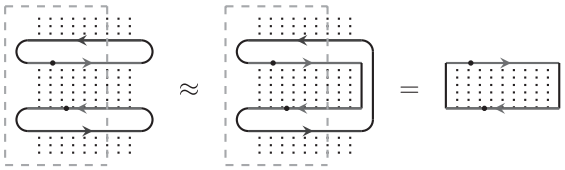

(6)

Here, the dots represent the insertion of Majorana operators, and the dashed boxes indicate the region in which Green's functions are the same. The Green's functions on the rhs exactly match those on the traditional Keldysh contour for the evolution of the density matrix of the single-sided steady state $\rho = 2^{-N/2}\mathcal{I}$ [36–38]. This result shows that in the long-time limit, the system is equivalent to two independently thermalized systems, each interacting with its respective infinite-temperature bath.

Consequently, the Green's function on $\mathcal{C}_{\text{red}}$ or $\mathcal{C}_{\text{blue}}$ matches the equilibrium Green's functions with $G^{bb}_{++} = -G^{aa}_{--} = \text{sgn}(\Delta u)G^{ba}_{+-} = -\text{sgn}(\Delta u)G^{ab}_{-+}$, and

$$G^{ba}_{+-} = \frac{1}{2}\left[\frac{A}{\cosh(B + A\mathcal{J}|\Delta u|)}\right]^{2/q}, \tag{7}$$

where $A = \cosh B$ and $\hat{\mu} = 2\mathcal{J}\sinh B$ are determined from the boundary conditions in Appendix B.

The remaining task involves computing the correlation between $\mathcal{C}_{\text{red}}$ and $\mathcal{C}_{\text{blue}}$ for long times. It is expected that this correlation will be localized around the boundary twists. As a representative example, we evaluate G^{aa}_{-+} [see Eq. (6)] with the understanding that other components can be derived by symmetry. Expanding $G^{aa}_{-+} = \frac{1}{2}(1 + g^{aa}_{-+}/q + \cdots)$, one arrives at the Liouville equation $\partial_u\partial_{u'}g^{aa}_{-+} = 2\mathcal{J}^2 e^{g^{aa}_{-+}}$. This equation is solved, as demonstrated in Appendix B, for the relevant boundary conditions. The resulting large-q analytical Green's function reads

$$G^{aa}_{-+} = \frac{1}{2}\left[\frac{A\text{csch}(A\mathcal{J}u)\text{csch}(A\mathcal{J}u' + B)}{\coth(A\mathcal{J}u' + B)[\coth(A\mathcal{J}u) + 2\tanh B] - 1}\right]^{2/q}.$$

This is depicted in Fig. 2(b), which shows a good agreement with the $q = 4$ numerical result. Furthermore, using the large-q solution, we show that the long-time entropy S is independent of $\mathcal{J}$ or $\hat{\mu}$ by computing $\partial_{\mathcal{J}}S = \partial_{\hat{\mu}}S = 0$, which is detailed in Appendix B. On the other hand, we expect $S = N\ln 2$ for $\hat{\mu}/\mathcal{J} \to \infty$ where the coupling to the bath dominates. We thus conclude $S = N\ln 2$ in the long-time limit for arbitrary $\mathcal{J}/\hat{\mu}$. Although we cannot obtain analytic results for intermediate times where the transition occurs, the simple extrapolation of the short- and long-time analytic results to intermediate times yields a time evolution of the purity very close to the large N numerical results obtained in the previous section.

C. Finite N trajectories

We now investigate whether signatures of replica wormholes are visible for finite N. The standard approach of duplicating the degrees of freedom of the original system using the Choi-Jamiolkowski isomorphism [78–81] is not viable in our case due to the presence of four time contours, which limit exact diagonalization up to $N \approx 6$. Instead, we exploit the Markovian properties of the Lindblad coupling which allows us to evolve only a single SYK. This is achieved by introducing quantum trajectories [82,83], which ensures that the coupling to the bath is considered even when replicas a and b are decoupled; see Fig. 1(d).

Specifically, we discretize time into small intervals with length δt. The evolution is determined by a random variable $\xi(u) \in (0,1)$ at time u,

$$\mathcal{U}_{\pm}(\delta t, \xi(u)) = \begin{cases} e^{\mp iH\delta t} & \text{if } \xi(u) > \delta p, \\ \sqrt{2}\chi_i & \text{if } \xi(u) < \delta p, \end{cases} \tag{8}$$

where the leakage probability is given by $\delta p = 1 - e^{-\mu N\delta t/2}$, indicating the probability of being detected and measured by the environment, i.e., experiencing a quantum jump. $\boldsymbol{\xi} = \{\xi(\delta t), \xi(2\delta t), \ldots, \xi(\mathcal{N}_t \cdot \delta t)\}$ then characterizes the full trajectory that determines the evolution operator and therefore defines the random quantum dynamics. Subsequently, $\text{Tr}(\mathcal{P}^2)$ is computed by substituting the connecting dots between forward/backward contours in Fig. 1(c) with identical, yet time-reversed, quantum trajectories. See Fig. 1(d) for a pictorial demonstration. After averaging over all possible trajectories, we arrive at $\text{Tr}(\mathcal{P}^2) = \overline{\mathcal{A}\cdot\mathcal{A}^*}$,

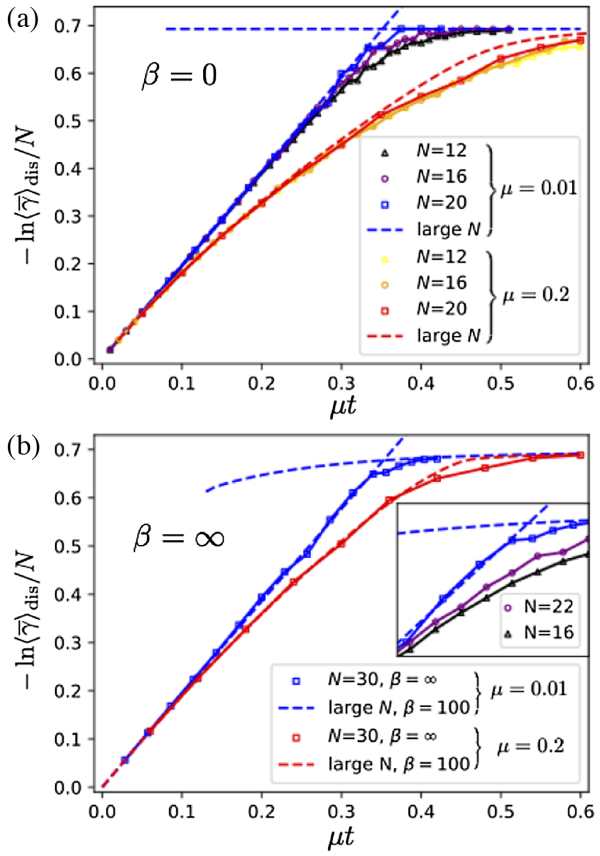

FIG. 4. Comparison between the numerical entropy growth at finite N computed by performing an average over quantum trajectories, and the previous large N results. We present results for (a) $\beta J = 0$ and (b) $\beta J = \infty$. Inset of (b) refers to the case of $N = 16, 22, 30$ at $\mu = 0.01J$ emphasized on the transition region.

where $\mathcal{A}$ denotes the amplitude in replica a, $\mathcal{A}^*$ is its time-reversed counterpart in replica b, and

$$\mathcal{A} = \mathrm{Tr}\big[\mathcal{U}_+(t,\boldsymbol{\xi}_{\rm L}^+)e^{-\beta H/2}\mathcal{U}_+(t,\boldsymbol{\xi}_{\rm R}^+) \cdot \mathcal{U}_-(t,\boldsymbol{\xi}_{\rm R}^-)e^{-\beta H/2}\mathcal{U}_-(t,\boldsymbol{\xi}_{\rm L}^-)\big]. \tag{9}$$

After normalization, the purity is determined using the above expression after averaging, denoted by $\bar{\gamma}$, over all trajectories.

We employ the Monte Carlo method to simulate [84,85] the infinitesimal random evolution, Eq. (8). This formalism makes possible the calculation of $\bar{\gamma}$ at $\beta J = 0$ and $\beta J = \infty$ up to $N = 20$ and $N = 30$, respectively. The results for the entropy growth shown in Fig. 4 for various values of μ exhibit excellent agreement with the large N calculation for the largest N we can explore numerically. We stress that for this largest N, the numerical results capture both the change in leading saddles for small μ and the termination of the first-order transition for $\mu \gtrsim \mu_c$. However, for smaller values of N, significant differences for intermediate times make it challenging to distinguish the transition from the crossover as μ increases. This observation confirms the crucial role of the quantum trajectory method, achieving a dramatic, up to fivefold, increase in system size, in order to reproduce the large N results. Our numerics confirms the possibility to observe entanglement dynamics with features of replica wormholes in quantum systems with moderate N, which makes more likely its experimental confirmation.

IV. CONCLUSION AND OUTLOOK

In this work, we delved into the dynamics of entanglement growth within a pair of dissipative SYK models. In the large N regime, we identified a first-order entanglement transition at low dissipation strengths. This phenomenon, absent in single dot SYK models [58], is attributed to the distinct types of Keldysh contours involved. Intriguingly, we observed that the long-time behavior closely mirrors replica wormholes within a gravitational context. Our analysis, particularly in the twisted replica space representation detailed in Appendix A, revealed the following process: Initially, the SYK systems exhibit high entanglement in L-R pairs. As they interact with their environment, either a sudden or gradual disentanglement occurs around the Page time, leading to the eventual establishment of entanglement with their respective environments. This transition depends on the strength of the environmental coupling, underscoring the monogamous nature of quantum entanglement [86,87] in dynamically evolving many-body systems. Furthermore, our numerical studies at finite N utilizing the quantum trajectories method indicate that the characteristics of the replica wormhole are observable even at moderate N values. This finding suggests potential for experimental investigation: With development of quantum technologies, the proposed mechanism of dynamical replica-symmetry breaking and its implications for entanglement [88–93] could be explored through digital quantum simulations [51,94–96] and in strongly interacting open quantum systems.

ACKNOWLEDGMENTS

We are grateful to A. Kamenev and Y. Gu for useful discussions. H. W., C. L., and A. M. G. G. acknowledge support from a National Key R&D Program of China (Project ID No. 2019YFA0308603). H. W. is also supported by NSFC Grant No. 12247131 and a Shanghai Super Postdoc Fellowship. A. M. G. G. also acknowledges partial support from a Shanghai talent program.

APPENDIX A: KELDYSH-LINDBLAD PATH INTEGRAL FOR PURITY

1. Contours and actions

The unitary evolution of the L-R system is governed by the Hamiltonian $H_{\rm S} = H_{\rm L} + H_{\rm R}$. For a given time t, the

wave function for the double-sided SYK system evolves according to

$$|\Psi(t)\rangle = e^{-\mathrm{i}H_S t}|\mathrm{TFD}_\beta\rangle = Z_\beta^{1/2} e^{-\mathrm{i}(H_\mathrm{L}+H_\mathrm{R})t} e^{-\beta(H_\mathrm{L}+H_\mathrm{R})/4}|I\rangle,$$

where the Majorana fermion on each side of the system satisfies $\chi_{i,\mathrm{L}}|I\rangle = -\mathrm{i}\chi_{i,\mathrm{R}}|I\rangle$. Under this convention, it is possible to map the double-sided SYK back to a single-sided SYK. The wave function projected onto a Majorana coherent state can be derived and represented as follows [57]:

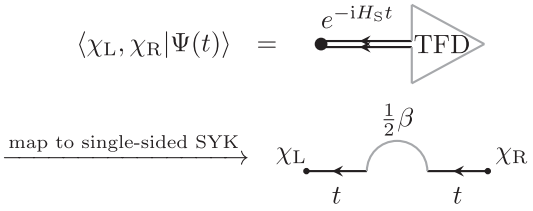

In the single-sided SYK picture, the L-R forward evolution is denoted by two left-pointing arrow lines $U_+ = e^{-\mathrm{i}Ht}$ separated by a semicircle that represents the imaginary evolution $U_{\beta/2} = e^{-\beta H/2}$. In the absence of any Lindbladian effects, one can define the corresponding unnormalized density matrix as $\mathcal{P}(t) = Z_\beta|\Psi(t)\rangle\langle\Psi(t)|$. Taking into account the conjugate part, one needs the backward evolution $U_- = e^{\mathrm{i}Ht}$, which is represented by a right-pointing arrow line. Thus, one can express the density matrix via the matrix element as

$\langle\chi_\mathrm{L},\chi_\mathrm{R}|\mathcal{P}(t)|\chi'_\mathrm{L},\chi'_\mathrm{R}\rangle$ =

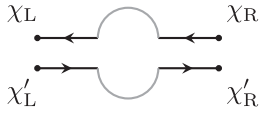

. (A1)

Here, the matrix element comprises four external legs: χ_L, χ_R as initial legs, and $\chi'_\mathrm{L}, \chi'_\mathrm{R}$ as final legs. This construction is distinct from the case of the one-sided SYK initialized in a thermal state, where the density matrix only contains two external legs [58].

When a Markovian environment is incorporated, as modeled by jump operators in the Lindblad formalism, it results in an effective coupling in the path integral between forward and backward contours at equal time. This originates from the left and right sides (which should not be confused with the L-R of the SYK systems, and should be denoted as $\pm$) of the density matrix $\mathcal{P}$. Within the infinitesimal time δt, the nonunitary equation of motion can be mapped to the path integral, provided the single-sided jump operators L_i are defined on the forward/backward contours as $L_{i,\pm}$. After integrating over a finite time on the contour of Eq. (A1) and identifying $L_{i,\pm}(s) = \chi_i(s_\pm)$, we attain the following contribution for the density matrix [36–38,74,75]:

$$\begin{aligned}\delta\mathcal{P}/\delta t &= \mu\sum_i\left[L_i\mathcal{P}L_i^\dagger - \frac{1}{2}\{L_i^\dagger L_i,\mathcal{P}\}\right]\\ &\to \exp\left[\int \delta t\,\mu\sum_i L_{i,+}L_{i,-}^\dagger - \frac{1}{2}L_{i,+}^\dagger L_{i,+} - \frac{1}{2}L_{i,-}^\dagger L_{i,-}\right]\\ &= \exp\left[\int ds\,\mu\sum_i \chi_i(s_+)\chi_i(s_-) - \mu N t\right].\end{aligned}$$

Here we use a time argument s to denote evolution, and s_+/s_- are equal time on the forward/backward branch. As a result, we can illustrate the density evolution of L-R systems with a Markovian reservoir as

$\mathcal{P}(t) =$

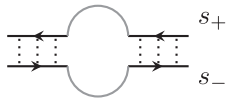

where the vertical dotted lines refer to the Lindblad couplings between forward/backward contours at equal time.

With knowledge of the density matrix at time t, the unnormalized purity $\mathrm{Tr}[\mathcal{P}(t)^2]$ can now be formulated by introducing two replicas, namely, 1 and 2. More specifically, in the basis of the Majorana coherent state, we can express the purity by linking the legs of two replicas so that the procedure is consistent with the operation of taking the trace [46,49], so $\mathrm{Tr}[\mathcal{P}\cdot\mathcal{P}]$ is equal to

$$\sum_{\chi\text{ in proper measure}} \overbrace{\langle\chi_\mathrm{L},\chi_\mathrm{R}|\mathcal{P}(t)|\chi'_\mathrm{L},\chi'_\mathrm{R}\rangle}^{\text{replica 1}} \underbrace{\langle\chi'_\mathrm{L},\chi'_\mathrm{R}|\mathcal{P}(t)|\chi_\mathrm{L},\chi_\mathrm{R}\rangle}_{\text{replica 2}}$$

=

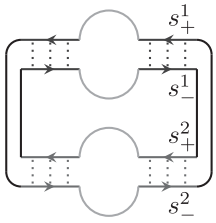

The TFD state leads to entanglement between the L-R systems. Hence, calculating the purity of this state results in a twisted link between the legs, which we depict in the diagram above. The presence of this twisted boundary condition between replicas 1 and 2 complicates the calculation of the purity. In particular, the definition of ∂_s, which typically arises in the path integral form $\chi(s)\partial_s\chi(s)$ to encode time ordering, becomes subtle to formulate at the twisting positions. Fortunately, there is a work-around that allows us to fix this issue. By reshuffling the time contour,

we can redefine new replicas denoted by a and b. This process is illustrated in the following diagram:

$$\mathrm{Tr}[\mathcal{P}(t)^2] \quad = \quad , \tag{A2}$$

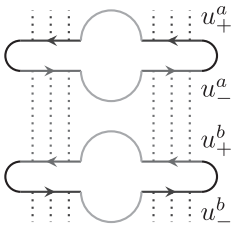

where the time domain along the contour $\mathcal{C}$ is denoted as $u \in [0, 8t + 4\beta]$, with the parametrization of forward (fwd), backward (bwd), and imaginary (img) contours as

$$\text{fwd}: \begin{cases} u^a_+ = u \in [0, t] \cup \left[t + \frac{1}{2}\beta, 2t + \frac{1}{2}\beta\right], \\ u^b_+ = u \in [4t + \beta, 5t + \beta] \cup \left[5t + \frac{3}{2}\beta, 6t + \frac{3}{2}\beta\right], \end{cases}$$

$$\text{bwd}: \begin{cases} u^a_- = u \in \left[2t + \frac{1}{2}\beta, 3t + \frac{1}{2}\beta\right] \cup [3t + \beta, 4t + \beta], \\ u^b_- = u \in \left[6t + \frac{3}{2}\beta, 7t + \frac{3}{2}\beta\right] \cup [7t + 2\beta, 8t + 2\beta], \end{cases}$$

$$\text{img}: u \in \left[t, t + \frac{1}{2}\beta\right] \cup \left[3t + \frac{1}{2}\beta, 3t + \beta\right] \cup \left[5t + \beta, 5t + \frac{3}{2}\beta\right] \cup \left[7t + \frac{3}{2}\beta, 7t + 2\beta\right].$$

Given the time domain u and the corresponding replicas a, b, it is straightforward to determine the time derivative operation ∂_u with respect to u. In the space of a, b, this operation is diagonal, represented as $\partial_u = G_0^{-1}$, where $G_0^{aa} = G_0^{bb} = \frac{1}{2}\mathrm{sgn}(u - u')$ and $G_0^{ab} = G_0^{ba} = 0$. This ∂_u also imposes the fermionic antiperiodic boundary condition in each replica automatically. The translation of this diagram Eq. (A2) back into the path integral representing the purity, results in

$$\mathrm{Tr}(\mathcal{P}^2) = \int \mathcal{D}\chi \, \exp\left\{ - \int_{\mathcal{C}} du \left[\frac{1}{2} \sum_i^N \chi_i \partial_u \chi_i + f(u) H \right] + \mu \sum_i^N \int du \left[\chi_i(u^a_+) \chi_i(u^b_-) + \chi_i(u^a_-) \chi_i(u^b_+) \right] - 2\mu N t \right\}.$$

The next step is to perform an average over disorder realizations, namely, the SYK random couplings $\langle \mathrm{Tr}(\mathcal{P}^2) \rangle_{\mathrm{dis}}$ and the definition of the Green's function $G(u, u') = \frac{1}{N} \sum_i \chi_i(u) \chi_i(u')$ and the corresponding Lagrange multiplier $\Sigma(u, u')$. This results in the following mth-effective action of $\langle \mathrm{Tr}(\mathcal{P}^m) \rangle_{\mathrm{dis}}$:

$$S^{(m)}_{\mathrm{eff}}[G, \Sigma] = -\frac{N}{2} \log \det(\partial_u - \Sigma) + \frac{N}{2} \int_{\mathcal{C}} du du' \left[\Sigma G - f(u) f(u') \frac{J^2}{q} G^q \right] - \frac{\mu N}{2} \int_{\mathcal{C}} du du' \, G(u, u') g(u, u') + m\mu N t,$$

where $f(u)$ and $g(u, u')$ stand for

$$f(u) = \begin{cases} \mathrm{i} & u \in \text{forward}, \\ -\mathrm{i} & u \in \text{backward}, \\ 1 & u \in \text{imaginary}, \end{cases}$$

$$g(u, u') = \begin{cases} +\delta(8t + 2\beta - u - u') & u \in \text{forward}, \\ -\delta(8t + 2\beta - u - u') & u \in \text{backward}. \end{cases} \tag{A3}$$

For $m = 2$, and in large N limit, we compute the path integral in the saddle-point approximation leading to $\mathrm{Tr}(\mathcal{P}^2) \simeq e^{-S^{(2)}_{\mathrm{eff}}[\mathcal{G}, \Sigma]}$, where $S^{(2)}_{\mathrm{eff}}[\mathcal{G}, \Sigma]$ is the on-shell action whose arguments follow the saddle points, usually termed Schwinger-Dyson, equations

$$\mathcal{G}(u, u') = \left[\partial_u - \Sigma(u, u')\right]^{-1},$$
$$\Sigma(u, u') = J^2 \mathcal{G}(u, u')^{q-1} f(u) f(u') + \mu g(u, u'). \tag{A4}$$

The normalization can be calculated by using the $m = 1$ single replica action, which eventually yields $Z_\beta = \mathrm{Tr}(\mathcal{P}) \simeq e^{-S^{(1)}_{\mathrm{eff}}}$. Finally, the Renyi entropy in the large N limit becomes $S = S^{(2)}_{\mathrm{eff}}[\mathcal{G}, \Sigma] - 2S^{(1)}_{\mathrm{eff}}[\mathcal{G}, \Sigma]$.

2. Solutions

The Schwinger-Dyson equations above are solved iteratively once the quantities G and Σ are discretized into a matrix form [24]. These equations are represented in two different replica spaces, a and b [46] and 1 and 2 (i.e., blue and red) [49], as illustrated in Fig. 5. The left and right panels display two distinct saddle-point solutions of Eq. (A4) calculated at the same time t. For early times, before the Page time where the transition occurs, the solution that is almost diagonal in the a, b space [left panel of Fig. 5(a)] exhibits lower entropy. However, for sufficiently long times, longer than the Page time, the solution which is nearly diagonal in the 1,2 space [right panel of Fig. 5(b)] tends to have a lower entropy. The physical interpretation of the process, when viewed from the 1,2 replica space representation, can be outlined as follows: Initially, L-R pairs of the SYKs are highly entangled, but under the impact of environmental interactions, they part ways and start entangling more intensively with their respective environments at the Page time. This illuminates the inherent monogamy feature of quantum entanglement [86,87].

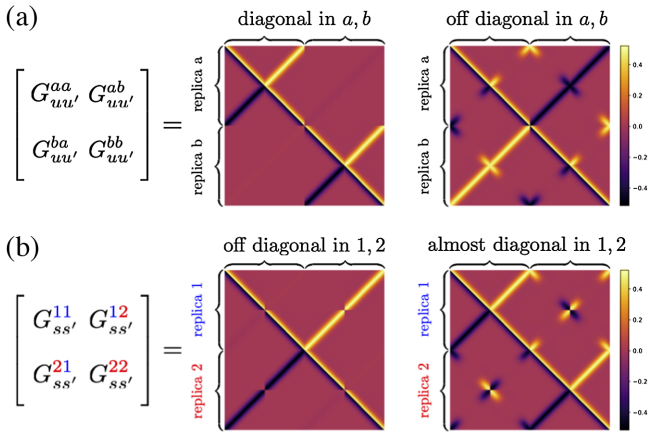

FIG. 5. Two distinct saddle-point solutions for Eq. (A4): replica diagonal vs replica off diagonal at time $t = 12/J$, with $\mu = 0.01J$ and $\beta = 0$. (a) $G(u, u')$ displayed in replica representations a and b. The left panel illustrates the replica-diagonal solution, while the right panel shows the replica-off-diagonal solution at the same time. (b) $G(s, s')$ presented in replica representations 1 and 2.

We have also calculated the growth of the purity for an initial TFD state at low temperature $\beta J = 100$. As is observed in Fig. 6(b), there is no qualitative difference between initial TFD states at low and high temperature.

APPENDIX B: THE LARGE-q SYK WITH DISSIPATION

1. Single-sided dissipative SYK

We provided additional details of analytical large-q calculation presented in the main text. Our starting point is a single-sided large-q SYK model with Hamiltonian

$$H = \sum_{1\le i_1<i_2<\ldots<i_q\le N} i^{q/2} J_{i_1 i_2 \ldots i_q} \chi_{i_1}\chi_{i_2}\cdots\chi_{i_q}.$$

$J_{i_1 i_2 \ldots i_q}$ with a different set of indices are independent Gaussian variables, with expectations and variances given by

$$\langle J_{i_1 i_2 \ldots i_q}\rangle_{\text{dis}} = 0,$$
$$\langle J^2_{i_1 i_2 \ldots i_q}\rangle_{\text{dis}} = \frac{(q-1)!J^2}{N^{q-1}} = \frac{2^{q-1}(q-1)!\mathcal{J}^2}{qN^{q-1}}.$$

We include a Markovian bath by considering the Lindblad master equation with jump operators $L_i = \sqrt{\mu}\chi_i$:

$$\partial_t \rho = -i[H,\rho] + \sum_i \mu\left(\chi_i \rho \chi_i - \frac{1}{2}\rho\right),$$

where ρ is the density matrix. Note that we employ a different notation for the density matrix from the one used in the main text, $\mathcal{P}$ where both L-R systems are considered. This model, and its solutions, are discussed in Refs. [36–38]. Here we just summarize these results for later use. A useful pictorial representation of the Keldysh contour at $\beta = 0$ is

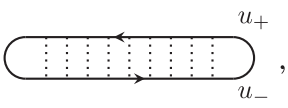

(B1)

where the solid arrow lines represent the branch with forward/backward evolution in time. The dotted lines represent the coupling induced by the environment. We focus on the time evolution toward the steady state with $\rho = 2^{-N/2}\mathcal{I}$. For that purpose, we compute the Green's functions $G_{\eta\eta'}(u, u')$. The Schwinger-Dyson equation reads

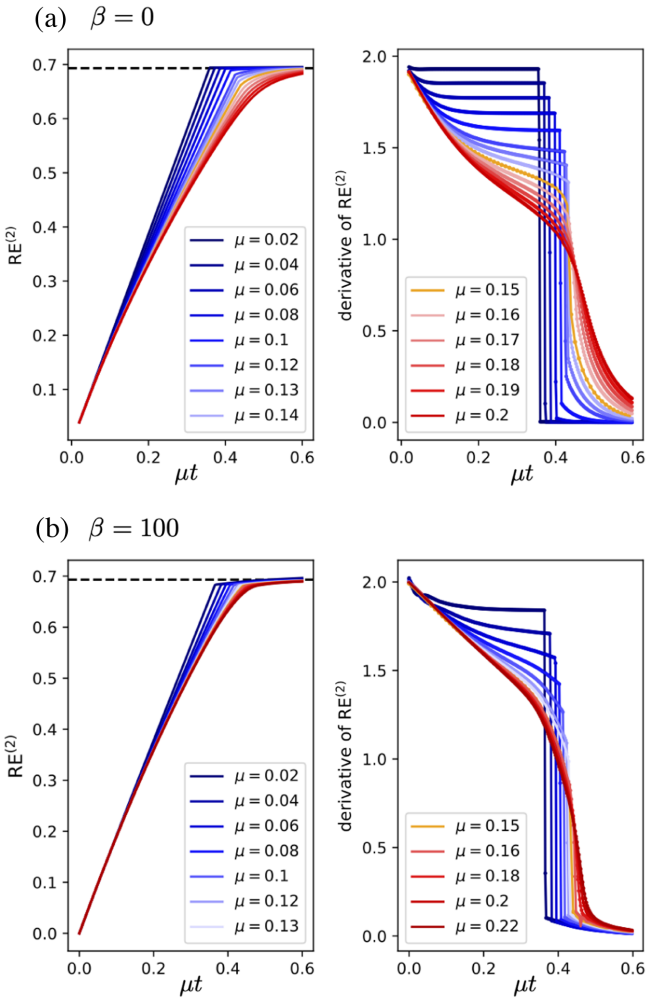

FIG. 6. (a) Left panel: large N Page curve for an initial $\beta J = 0$ TFD state, for values of the coupling to the bath μ ranging from $0.02J$ to $0.2J$. Right panel: time dependence of the derivative of the Rényi entropy for different values of μ as a function of the rescaled time μt. (b) Large N Page curve for an initial $\beta J = 100$ TFD state.

$$\begin{pmatrix} \partial_u - \Sigma_{++} & \mu - \Sigma_{+-} \\ -\mu - \Sigma_{-+} & -\partial_u - \Sigma_{--} \end{pmatrix} \circ \begin{pmatrix} G_{++} & G_{+-} \\ G_{-+} & G_{--} \end{pmatrix} = \hat{I},$$
$$\Sigma_{\eta\eta'} = -\eta\eta' \frac{\mathcal{J}^2}{q} (2G_{\eta\eta'})^{q-1}.$$

We introduce $\mu = \hat{\mu}/q$ and fix $\hat{\mu}$ in the large-q limit. At $q = \infty$, both μ and Σ become zero. Consequently, the Green's functions read

$$G_{0,++} = -G_{0,--} = \frac{1}{2}\mathrm{sgn}(u - u') = \frac{1}{2}\mathrm{sgn}(\Delta u),$$
$$G_{0,-+} = -G_{0,+-} = \frac{1}{2}. \tag{B2}$$

This is the Green's function of free Majorana fermions, which serves as a good first approximation in the large-q limit [24,97]. We then expand $G_{\eta\eta'} = G_{0,\eta\eta'}(1 + g_{\eta\eta'}/q + \cdots)$ in the large-q limit. In Majorana systems, we can focus on G_{-+}, which determines all other Green's functions due to the symmetry of the Keldysh contour. Keeping only the leading $1/q$ corrections, the Schwinger-Dyson equation for G_{-+} becomes

$$\partial_u \partial_{u'} g_{-+} = 2\mathcal{J}^2 e^{g_{-+}} + 2\hat{\mu}\delta(\Delta u). \tag{B3}$$

We first focus on $u > u'$, where Eq. (B3) becomes a Liouville equation. The translational invariant solution reads

$$e^{g_{-+}} = \frac{A^2}{\cosh^2(B + A\mathcal{J}\Delta u)} \tag{B4}$$

for $\Delta u > 0$. Because of the reflection symmetry of the Keldysh contour with initial density matrix $\rho = 2^{-N/2}\mathcal{I}$, we have $g_{-+}(\Delta u) = g_{-+}(-\Delta u)$. Parameters A and B are determined from the boundary condition at $t = 0$,

$$g(0) = 0, \qquad \partial_u g(0^+) = -\hat{\mu}.$$

The first boundary condition comes from $\chi^2 = 1/2$, and the second boundary condition takes into account the last term in Eq. (B3), which results in

$$A = \cosh B, \qquad \hat{\mu} = 2\mathcal{J}\sinh B. \tag{B5}$$

In the special limit $\hat{\mu} \to 0$, we find $B = 0$ and $A = 1$.

2. The purity calculation

Now we turn to the purity calculation involving two copies of the density matrix investigated in the main text. For $\beta = 0$, the Keldysh contour with time $2t$ becomes

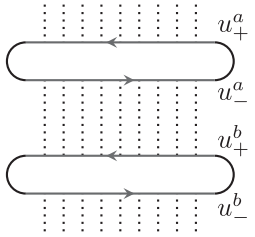

(B6)

The Schwinger-Dyson equation on this doubled Keldysh contour reads

$$\sum_{p''} \begin{pmatrix} \delta^{pp''}\partial_u - \Sigma^{pp''}_{++} & \mu\delta^{\bar{p}p'} - \Sigma^{pp''}_{+-} \\ -\mu\delta^{\bar{p}p'} - \Sigma^{pp''}_{-+} & -\delta^{pp''}\partial_u - \Sigma^{pp''}_{--} \end{pmatrix} \circ \begin{pmatrix} G^{p''p'}_{++} & G^{p''p'}_{+-} \\ G^{p''p'}_{-+} & G^{p''p'}_{--} \end{pmatrix} = \hat{I},$$
$$\Sigma^{pp'}_{\eta\eta'} = -\eta\eta' \frac{\mathcal{J}^2}{q} (2G^{pp'}_{\eta\eta'})^{q-1}, \tag{B7}$$

where $p, p', p'' \in \{a, b\}$, and $\bar{p} \neq p$. The large-q saddle-point equation can be derived after specifying $G^{pp'}_{0,\eta\eta'}$ with $\eta, \eta' = \pm$, which also takes the form of the Liouville equation with delta function sources. However, comparing to the single-sided calculation, there are two main difficulties: (1) Unlike Eq. (B1), the boundary condition in Eq. (B6) breaks the time translation symmetry, so there is no a simple way to find analytical solutions. (2) The $G^{pp'}_{0,\eta\eta'}$ takes a different form in the short-time/long-time regime, as in the eternal traversable wormhole calculation [30]. In the following sections, we focus on the short-time limit and the long-time limit separately, where the Green's functions are almost translation invariant.

a. Short-time solution

For sufficiently short times $\hat{\mu}t \ll q$, the contribution due to a finite μ is perturbative. To leading order in $\hat{\mu}/\mathcal{J}$, the Green's function within each replica a/b can be approximated by the equilibrium solution with $\hat{\mu} = 0$. Keeping to the $1/q$ order, the result reads [24]

$$G^D_{\eta\eta'}(u, u') = \langle \chi^{a/b}_\eta(u)\chi^{a/b}_{\eta'}(u')\rangle = \frac{G_{0,\eta\eta'}(\Delta u)}{\cosh^{2/q}(\mathcal{J}\Delta u)}.$$

For the inter-replica Green's functions, the result can be computed by solving Eq. (B7) perturbatively in μ. We find

$$G^{ba}_{\eta\eta'}(u, u') = \langle \chi^b_\eta(u)\chi^a_{\eta'}(u')\rangle = \quad \eta' \xrightarrow{\ \mu\ } \eta$$
$$\approx \frac{\hat{\mu}}{q}\sum_\zeta \int_0^{2t} du'' G^D_{\eta\zeta}(u, u'')G^D_{-\zeta\eta'}(u'', u').$$

To $1/q$ order, we can replace $G^D_{\eta\eta'}$ by $G_{0,\eta\eta'}$. The result reads

$$G^{ba}_{\eta\eta'}(u,u') = \frac{\hat{\mu}}{2q}\begin{pmatrix} u+u'-2t & 2t-|u-u'| \\ 2t-|u-u'| & u+u'-2t \end{pmatrix}, \tag{B8}$$

where $u, u' \in [0, 2t]$. We find off-diagonal components are of the order $\hat{\mu}t/q$. It becomes large enough at sufficient long time $t \sim q$, where our perturbation results breakdown. By computing the on-shell action, it is straightforward to show that Eq. (B8) results in $S \approx 2\hat{\mu}Nt/q$ for short time.

b. Long-time solution

At long times, the pairing between branches changes, and the solution is highly replica off diagonal. In the long-time limit $\hat{\mu}t \to \infty$, the Green's functions can be approximated by the "factorization of twist operators":

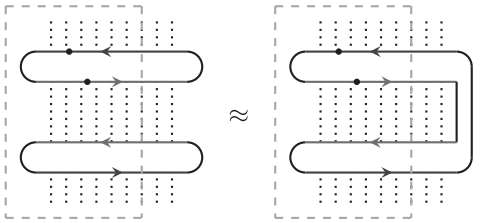

(B9)

Here the dots represent the insertion of Majorana operators, and the dashed box indicates the region in which Green's functions are the same. Green's functions on the rhs can be computed analytically. We first consider the Green's functions where two fermion operators are inserted on branches $C_{\text{red}} = (b,+) \cup (a,-)$. By contracting the redundant branches, we find

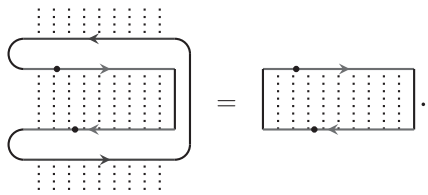

(B10)

This is exactly the Keldysh contour Eq. (B1) for the evolution of the density matrix. Consequently, the Green's function on C_{red} matches the equilibrium Green's functions Eqs. (B4) and (B5) with finite $\hat{\mu}$:

$$\begin{aligned} G^{bb}_{++} &= -G^{aa}_{--} = \frac{1}{2}\text{sgn}(\Delta u)\left[\frac{A}{\cosh(B+A\mathcal{J}|\Delta u|)}\right]^{2/q}, \\ G^{ba}_{+-} &= -G^{ab}_{-+} = \frac{1}{2}\left[\frac{A}{\cosh(B+A\mathcal{J}|\Delta u|)}\right]^{2/q}. \end{aligned} \tag{B11}$$

Similar solutions hold on branches $C_{\text{blue}} = (b,-) \cup (a,+)$.

The remaining task is to compute the correlation between C_{blue} and C_{red}. We take the two-point function illustrated in Eq. (B9) as an example, while other components can be obtained straightforwardly. As in the previous calculations, we expand $G^{aa}_{-+} = \frac{1}{2}(1 + g^{aa}_{-+}/q + \cdots)$, and the equation satisfied by g^{aa}_{-+} is again of Liouville type,

$$\partial_u \partial_{u'} g^{aa}_{-+} = 2\mathcal{J}^2 e^{g^{aa}_{-+}}. \tag{B12}$$

However, unlike Eq. (B3), there is no source term induced by the environment. As we will see, this leads to a decay of $g^{aa}_{-+}(u,u')$ when u and u' are away from 0.

The general solution to the Liouville equation Eq. (B12) can be written as

$$e^{g^{aa}_{-+}(u,u')} = -\frac{\mathcal{F}_1'(\mathcal{J}u)\mathcal{F}_2'(\mathcal{J}u')}{[\mathcal{F}_1(\mathcal{J}u) - \mathcal{F}_2(\mathcal{J}u')]^2} \tag{B13}$$

for arbitrary functions $(\mathcal{F}_1, \mathcal{F}_2)$. Using the previous boundary condition at $t = 0$, we have $(u > 0)$,

$$e^{g^{aa}_{-+}(0,u)} = e^{g^{aa}_{-+}(u,0)} = \frac{A^2}{\cosh^2(B + A\mathcal{J}u)}. \tag{B14}$$

Combining Eqs. (B13) and (B14), we obtain

$$\begin{aligned} \mathcal{F}_1(x) &= \frac{1}{A\coth(Ax) + 2A\tanh B}, \\ \mathcal{F}_2(x) &= \frac{\coth(B+Ax)}{A}. \end{aligned}$$

This gives $G^{aa}_{-+} = e^{g^{aa}_{-+}/q}/2$ with

$$e^{g^{aa}_{-+}} = \frac{A^2\text{csch}^2(A\mathcal{J}u)\text{csch}^2(A\mathcal{J}u'+B)}{\{\coth(A\mathcal{J}u'+B)[\coth(A\mathcal{J}u) + 2\tanh B] - 1\}^2}, \tag{B15}$$

which determines the correlation between C_{blue} and C_{red}. We observed the expected exponential decay for $\mathcal{J}u \gg 1$.

Furthermore, using the large-q solution, we show that the long-time entropy $S = S^{(2)}_{\text{eff}}[\mathcal{G},\Sigma] - 2S^{(1)}_{\text{eff}}[\mathcal{G},\Sigma]$ is independent of $\mathcal{J}$ or $\hat{\mu}$ by computing its derivative with respect to these variables $\partial_{\mathcal{J}} S = \partial_{\hat{\mu}} S = 0$. Since $S^{(1)}_{\text{eff}} = \text{Tr}(\mathcal{P}) = Z_\beta = 2^{N/2}$ for $\beta = 0$, we focus on $\partial_{\mathcal{J}} S^{(2)}_{\text{eff}}$ and $\partial_{\hat{\mu}} S^{(2)}_{\text{eff}}$. Explicitly, we have

$$\begin{aligned} \partial_{\mathcal{J}} S^{(2)}_{\text{eff}}[\mathcal{G},\Sigma] &= -\frac{N\mathcal{J}}{2q^2}\int_{\mathcal{C}} du du'\, f(u)f(u')|2G(u,u')|^q \\ &= -\frac{N\mathcal{J}}{2q^2}\int_{\mathcal{C}} du du'\, f(u)f(u')e^{g(u,u')}. \end{aligned} \tag{B16}$$

Here we omit the a/b and $\pm$ labels for simplicity. Since Eq. (B16) is local in time, Eqs. (B11) and (B15) contribute separately. The contribution from Eq. (B11) is zero. This is because it matches the on-shell action of the single-sided contour Eq. (B10). On the other hand, we know that the

on-shell action of the single-sided contour is time independent due to the unitarity. Mathematically, this originates from the cancellation between contributions of $(G^{ab}_{-+}, G^{ba}_{+-})$ and $(G^{aa}_{--}, G^{bb}_{++})$, which takes different sign factors $f(u)f(u')$. Closer examination reveals similar cancellations exist for contributions from Eq. (B15). As a result, we find $\partial_{\mathcal{J}} S^{(2)}_{\text{eff}} = 0$. We then compute

$$\partial_{\hat{\mu}} S^{(2)}_{\text{eff}}[\mathcal{G}, \Sigma] = -\frac{N}{2q}\int_{\mathcal{C}} du du' G(u,u') g(u,u') + \frac{mNt}{q}. \tag{B17}$$

Following Eq. (A3), $g(u,u')$ is a combination of Dirac delta functions. As a result, Eq. (B17) only depends on $G^{ba}_{+-}(0) = -G^{ab}_{-+}(0) = 1/2$, which gives $\partial_{\hat{\mu}} S^{(2)}_{\text{eff}} = 0$. Finally, we expect $S = N \ln 2$ for $\hat{\mu}/\mathcal{J} \to \infty$ where the coupling to bath dominates. We thus conclude $S = N \ln 2$ in the long-time limit for arbitrary $\mathcal{J}/\hat{\mu}$.

[1] A. Guo, G. J. Salamo, D. Duchesne, R. Morandotti, M. Volatier-Ravat, V. Aimez, G. A. Siviloglou, and D. N. Christodoulides, Observation of $\mathcal{PT}$-symmetry breaking in complex optical potentials, Phys. Rev. Lett. **103**, 093902 (2009).

[2] J. Li, A. K. Harter, J. Liu, L. de Melo, Y. N. Joglekar, and L. Luo, Observation of parity-time symmetry breaking transitions in a dissipative Floquet system of ultracold atoms, Nat. Commun. **10**, 855 (2019).

[3] K. Kawabata, Y. Ashida, and M. Ueda, Information retrieval and criticality in parity-time-symmetric systems, Phys. Rev. Lett. **119**, 190401 (2017).

[4] K. Kawabata, Y. Ashida, H. Katsura, and M. Ueda, Parity-time-symmetric topological superconductor, Phys. Rev. B **98**, 085116 (2018).

[5] J. Wiersig, Enhancing the sensitivity of frequency and energy splitting detection by using exceptional points: Application to microcavity sensors for single-particle detection, Phys. Rev. Lett. **112**, 203901 (2014).

[6] L.-J. Zhai and S. Yin, Out-of-time-ordered correlator in non-Hermitian quantum systems, Phys. Rev. B **102**, 054303 (2020).

[7] A. M. García-García, L. Sá, and J. J. M. Verbaarschot, Universality and its limits in non-Hermitian many-body quantum chaos using the Sachdev-Ye-Kitaev model, Phys. Rev. D **107**, 066007 (2023).

[8] J. Li, T. Prosen, and A. Chan, Spectral statistics of non-Hermitian matrices and dissipative quantum chaos, Phys. Rev. Lett. **127**, 170602 (2021).

[9] Z. Xu, A. Chenu, T. Prosen, and A. del Campo, Thermofield dynamics: Quantum chaos versus decoherence, Phys. Rev. B **103**, 064309 (2021).

[10] J. Cornelius, Z. Xu, A. Saxena, A. Chenu, and A. del Campo, Spectral filtering induced by non-Hermitian evolution with balanced gain and loss: Enhancing quantum chaos, Phys. Rev. Lett. **128**, 190402 (2022).

[11] Z. Xu, L. P. García-Pintos, A. Chenu, and A. Del Campo, Extreme decoherence and quantum chaos, Phys. Rev. Lett. **122**, 014103 (2019).

[12] K. Kawabata, K. Shiozaki, M. Ueda, and M. Sato, Symmetry and topology in non-Hermitian physics, Phys. Rev. X **9**, 041015 (2019).

[13] A. M. García-García, L. Sá, and J. J. M. Verbaarschot, Symmetry classification and universality in non-Hermitian many-body quantum chaos by the Sachdev-Ye-Kitaev model, Phys. Rev. X **12**, 021040 (2022).

[14] K. Kawabata, A. Kulkarni, J. Li, T. Numasawa, and S. Ryu, Symmetry of open quantum systems: Classification of dissipative quantum chaos, PRX Quantum **4**, 030328 (2023).

[15] L. Sá, P. Ribeiro, and T. Prosen, Symmetry classification of many-body Lindbladians: Tenfold way and beyond, Phys. Rev. X **13**, 031019 (2023).

[16] Y. Li, X. Chen, and M. P. A. Fisher, Quantum Zeno effect and the many-body entanglement transition, Phys. Rev. B **98**, 205136 (2018).

[17] B. Skinner, J. Ruhman, and A. Nahum, Measurement-induced phase transitions in the dynamics of entanglement, Phys. Rev. X **9**, 031009 (2019).

[18] A. Chan, R. M. Nandkishore, M. Pretko, and G. Smith, Unitary-projective entanglement dynamics, Phys. Rev. B **99**, 224307 (2019).

[19] S. Choi, Y. Bao, X.-L. Qi, and E. Altman, Quantum error correction in scrambling dynamics and measurement-induced phase transition, Phys. Rev. Lett. **125**, 030505 (2020).

[20] Z. Weinstein, S. P. Kelly, J. Marino, and E. Altman, Scrambling transition in a radiative random unitary circuit, Phys. Rev. Lett. **131**, 220404 (2023).

[21] P. Zhang and Z. Yu, Dynamical transition of operator size growth in quantum systems embedded in an environment, Phys. Rev. Lett. **130**, 250401 (2023).

[22] S. Sachdev and J. Ye, Gapless spin-fluid ground state in a random quantum Heisenberg magnet, Phys. Rev. Lett. **70**, 3339 (1993).

[23] A. Kitaev, A simple model of quantum holography, in *Proceedings the KITP Program: Entanglement in Strongly-Correlated Quantum Matter, 2015*, http://online.kitp.ucsb.edu/online/entangled15/.

[24] J. Maldacena and D. Stanford, Remarks on the Sachdev-Ye-Kitaev model, Phys. Rev. D **94**, 106002 (2016).
[25] A. Kitaev and S. J. Suh, The soft mode in the Sachdev-Ye-Kitaev model and its gravity dual, J. High Energy Phys. 05 (2018) 183.
[26] R. Jackiw, Lower dimensional gravity, Nucl. Phys. **B252**, 343 (1985).
[27] C. Teitelboim, Gravitation and Hamiltonian structure in two spacetime dimensions, Phys. Lett. **126B**, 41 (1983).
[28] A. Almheiri and J. Polchinski, Models of AdS_2 backreaction and holography, J. High Energy Phys. 11 (2015) 014.
[29] J. Maldacena, D. Stanford, and Z. Yang, Conformal symmetry and its breaking in two-dimensional nearly anti–de Sitter space, Prog. Theor. Exp. Phys. **2016**, 12C104 (2016).
[30] J. Maldacena and X.-L. Qi, Eternal traversable wormhole, arXiv:1804.00491.
[31] S. Plugge, E. Lantagne-Hurtubise, and M. Franz, Revival dynamics in a traversable wormhole, Phys. Rev. Lett. **124**, 221601 (2020).
[32] P. Saad, S. H. Shenker, and D. Stanford, A semiclassical ramp in SYK and in gravity, arXiv:1806.06840.
[33] X.-L. Qi and P. Zhang, The coupled SYK model at finite temperature, J. High Energy Phys. 05 (2020) 129.
[34] A. M. García-García and V. Godet, Euclidean wormhole in the Sachdev-Ye-Kitaev model, Phys. Rev. D **103**, 046014 (2021).
[35] A. M. García-García, Y. Jia, D. Rosa, and J. J. M. Verbaarschot, Dominance of replica off-diagonal configurations and phase transitions in a *PT* symmetric Sachdev-Ye-Kitaev model, Phys. Rev. Lett. **128**, 081601 (2022).
[36] A. Kulkarni, T. Numasawa, and S. Ryu, Lindbladian dynamics of the Sachdev-Ye-Kitaev model, Phys. Rev. B **106**, 075138 (2022).
[37] K. Kawabata, A. Kulkarni, J. Li, T. Numasawa, and S. Ryu, Dynamical quantum phase transitions in Sachdev-Ye-Kitaev Lindbladians, Phys. Rev. B **108**, 075110 (2023).
[38] A. M. García-García, L. Sá, J. J. M. Verbaarschot, and J. P. Zheng, Keldysh wormholes and anomalous relaxation in the dissipative Sachdev-Ye-Kitaev model, Phys. Rev. D **107**, 106006 (2023).
[39] L. Sá, P. Ribeiro, and T. Prosen, Lindbladian dissipation of strongly-correlated quantum matter, Phys. Rev. Res. **4**, L022068 (2022).
[40] B. Bhattacharjee, X. Cao, P. Nandy, and T. Pathak, Operator growth in open quantum systems: Lessons from the dissipative SYK, J. High Energy Phys. 03 (2023) 054.
[41] S. W. Hawking, Black holes and thermodynamics, Phys. Rev. D **13**, 191 (1976).
[42] S. Ryu and T. Takayanagi, Holographic derivation of entanglement entropy from the anti–de Sitter space/conformal field theory correspondence, Phys. Rev. Lett. **96**, 181602 (2006).
[43] S. Ryu and T. Takayanagi, Aspects of holographic entanglement entropy, J. High Energy Phys. 08 (2006) 045.
[44] A. Lewkowycz and J. Maldacena, Aspects of holographic entanglement entropy, J. High Energy Phys. 08 (2013) 090.
[45] A. Almheiri, T. Hartman, J. Maldacena, E. Shaghoulian, and A. Tajdini, Replica wormholes and the entropy of Hawking radiation, J. High Energy Phys. 05 (2020) 013.
[46] G. Penington, S. H. Shenker, D. Stanford, and Z. Yang, Replica wormholes and the black hole interior, J. High Energy Phys. 03 (2022) 205.
[47] A. Almheiri, T. Hartman, J. Maldacena, E. Shaghoulian, and A. Tajdini, The entropy of Hawking radiation, Rev. Mod. Phys. **93**, 035002 (2021).
[48] D. N. Page, Information in black hole radiation, Phys. Rev. Lett. **71**, 3743 (1993).
[49] Y. Chen, X.-L. Qi, and P. Zhang, Replica wormhole and information retrieval in the SYK model coupled to Majorana chains, J. High Energy Phys. 06 (2020) 121.
[50] Z. Luo, Y.-Z. You, J. Li, C.-M. Jian, D. Lu, C. Xu, B. Zeng, and R. Laflamme, Quantum simulation of the non-Fermi-liquid state of Sachdev-Ye-Kitaev model, npj Quantum Inf. **5**, 53 (2019).
[51] D. Jafferis, A. Zlokapa, J. D. Lykken, D. K. Kolchmeyer, S. I. Davis, N. Lauk, H. Neven, and M. Spiropulu, Traversable wormhole dynamics on a quantum processor, Nature (London) **612**, 51 (2022).
[52] H. Wang, D. Bagrets, A. L. Chudnovskiy, and A. Kamenev, On the replica structure of Sachdev-Ye-Kitaev model, J. High Energy Phys. 09 (2019) 057.
[53] Y. Chen, H. Zhai, and P. Zhang, Tunable quantum chaos in the Sachdev-Ye-Kitaev model coupled to a thermal bath, J. High Energy Phys. 07 (2017) 150.
[54] P. Zhang, Evaporation dynamics of the Sachdev-Ye-Kitaev model, Phys. Rev. B **100**, 245104 (2019).
[55] A. Almheiri, A. Milekhin, and B. Swingle, Universal constraints on energy flow and SYK thermalization, arXiv:1912.04912.
[56] W. Israel, Thermo field dynamics of black holes, Phys. Lett. **57A**, 107 (1976).
[57] Y. Gu, A. Lucas, and X.-L. Qi, Spread of entanglement in a Sachdev-Ye-Kitaev chain, J. High Energy Phys. 09 (2017) 120.
[58] K. Su, P. Zhang, and H. Zhai, Page curve from non-Markovianity, J. High Energy Phys. 06 (2021) 156.
[59] P. Zhang, Entanglement entropy and its quench dynamics for pure states of the Sachdev-Ye-Kitaev model, J. High Energy Phys. 06 (2020) 143.
[60] A. Haldar, S. Bera, and S. Banerjee, Rényi entanglement entropy of Fermi and non-Fermi liquids: Sachdev-Ye-Kitaev model and dynamical mean field theories, Phys. Rev. Res. **2**, 033505 (2020).
[61] Y. Chen, Entropy linear response theory with non-Markovian bath, J. High Energy Phys. 04 (2021) 215.
[62] Y. Chen and P. Zhang, Entanglement entropy of two coupled SYK models and eternal traversable wormhole, J. High Energy Phys. 07 (2019) 033.
[63] P. Dadras and A. Kitaev, Perturbative calculations of entanglement entropy, J. High Energy Phys. 03 (2021) 198.
[64] S.-K. Jian and B. Swingle, Phase transition in von Neumann entanglement entropy from replica symmetry breaking, J. High Energy Phys. 11 (2023) 221.
[65] P. Dadras, Disentangling the thermofield-double state, J. High Energy Phys. 01 (2022) 075.
[66] P. Zhang, Information scrambling and entanglement dynamics of complex Brownian Sachdev-Ye-Kitaev models, J. High Energy Phys. 04 (2023) 105.

[67] S.-K. Jian, C. Liu, X. Chen, B. Swingle, and P. Zhang, Measurement-induced phase transition in the monitored Sachdev-Ye-Kitaev model, Phys. Rev. Lett. **127**, 140601 (2021).
[68] C. Liu, P. Zhang, and X. Chen, Non-unitary dynamics of Sachdev-Ye-Kitaev chain, SciPost Phys. **10**, 048 (2021).
[69] P. Zhang, S.-K. Jian, C. Liu, and X. Chen, Emergent replica conformal symmetry in non-Hermitian SYK_2 chains, Quantum **5**, 579 (2021).
[70] A. Milekhin and F. K. Popov, Measurement-induced phase transition in teleportation and wormholes, arXiv:2210.03083.
[71] T.-G. Zhou, Y.-N. Zhou, and P. Zhang, Full counting statistics across the entanglement phase transition of non-Hermitian Hamiltonians with charge conservation, Phys. Rev. B **108**, 094308 (2023).
[72] Y. Gu, A. Kitaev, S. Sachdev, and G. Tarnopolsky, Notes on the complex Sachdev-Ye-Kitaev model, J. High Energy Phys. 02 (2020) 157.
[73] C. L. Baldwin and B. Swingle, Quenched vs annealed: Glassiness from SK to SYK, Phys. Rev. X **10**, 031026 (2020).
[74] A. Kamenev, *Field Theory of Non-Equilibrium Systems* (Cambridge University Press, Cambridge, England, 2023).
[75] L. M. Sieberer, M. Buchhold, and S. Diehl, Keldysh field theory for driven open quantum systems, Rep. Prog. Phys. **79**, 096001 (2016).
[76] F. Thompson and A. Kamenev, Field theory of many-body Lindbladian dynamics, Ann. Phys. (Amsterdam) **455**, 169385 (2023).
[77] A. Almheiri, R. Mahajan, and J. Maldacena, Islands outside the horizon, arXiv:1910.11077.
[78] J. E. Tyson, Operator-Schmidt decompositions and the Fourier transform, with applications to the operator-Schmidt numbers of unitaries, J. Phys. A **36**, 10101 (2003).
[79] M. Zwolak and G. Vidal, Mixed-state dynamics in one-dimensional quantum lattice systems: A time-dependent superoperator renormalization algorithm, Phys. Rev. Lett. **93**, 207205 (2004).
[80] T. Prosen, Third quantization: A general method to solve master equations for quadratic open Fermi systems, New J. Phys. **10**, 043026 (2008).
[81] Y.-N. Zhou, L. Mao, and H. Zhai, Rényi entropy dynamics and Lindblad spectrum for open quantum systems, Phys. Rev. Res. **3**, 043060 (2021).
[82] K. Mølmer, Y. Castin, and J. Dalibard, Monte Carlo wave-function method in quantum optics, J. Opt. Soc. Am. B **10**, 524 (1993).
[83] H. M. Wiseman, Quantum trajectories and quantum measurement theory, J. Eur. Opt. Soc. B **8**, 205 (1996).
[84] A. M. García-García, C. Liu, and J. J. M. Verbaarschot, Sparsity independent Lyapunov exponent in the Sachdev-Ye-Kitaev model, arXiv:2311.00639.
[85] C. Liu, REAPERS: A REAsonably PERformant simulator for qubit systems, https://github.com/cl91/REAPERS, 2023.
[86] V. Coffman, J. Kundu, and W. K. Wootters, Distributed entanglement, Phys. Rev. A **61**, 052306 (2000).
[87] T. J. Osborne and F. Verstraete, General monogamy inequality for bipartite qubit entanglement, Phys. Rev. Lett. **96**, 220503 (2006).
[88] T. Schuster, B. Kobrin, P. Gao, I. Cong, E. T. Khabiboulline, N. M. Linke, M. D. Lukin, C. Monroe, B. Yoshida, and N. Y. Yao, Many-body quantum teleportation via operator spreading in the traversable wormhole protocol, Phys. Rev. X **12**, 031013 (2022).
[89] A. R. Brown, H. Gharibyan, S. Leichenauer, H. W. Lin, S. Nezami, G. Salton, L. Susskind, B. Swingle, and M. Walter, Quantum gravity in the lab. I. Teleportation by size and traversable wormholes, PRX Quantum **4**, 010320 (2023).
[90] S. Nezami, H. W. Lin, A. R. Brown, H. Gharibyan, S. Leichenauer, G. Salton, L. Susskind, B. Swingle, and M. Walter, Quantum gravity in the lab. II. Teleportation by size and traversable wormholes, PRX Quantum **4**, 010321 (2023).
[91] H.-Y. Huang, R. Kueng, and J. Preskill, Predicting many properties of a quantum system from very few measurements, Nat. Phys. **16**, 1050 (2020).
[92] A. Elben, B.Vermersch, R. van Bijnen, C. Kokail, T. Brydges, C. Maier, M. K. Joshi, R. Blatt, C. F. Roos, and P. Zoller, Cross-platform verification of intermediate scale quantum devices, Phys. Rev. Lett. **124**, 010504 (2020).
[93] A. Rath, R. van Bijnen, A. Elben, P. Zoller, and B. Vermersch, Importance sampling of randomized measurements for probing entanglement, Phys. Rev. Lett. **127**, 200503 (2021).
[94] Google Quantum AI *et al.*, Measurement-induced entanglement and teleportation on a noisy quantum processor, Nature (London) **622**, 481 (2023).
[95] M. McGinley, S. Leontica, S. J. Garratt, J. Jovanovic, and S. H. Simon, Quantifying information scrambling via classical shadow tomography on programmable quantum simulators, Phys. Rev. A **106**, 012441 (2022).
[96] Bluvstein *et al.*, Logical quantum processor based on reconfigurable atom arrays, Nature (London) **626**, 58 (2024).
[97] D. A. Roberts, D. Stanford, and A. Streicher, Operator growth in the SYK model, J. High Energy Phys. 06 (2018) 122.